The value of satellite remote sensing soil moisture data and the DISPATCH algorithm in irrigation fields

Mireia Fontanet[1,2,3], Daniel Fernàndez-Garcia[2,3], Francesc Ferrer[1]

[1]LabFerrer, Cervera, 25200, Spain

5   [2]Department of Civil and Environmental Engineering, Universitat Politècnica de Catalunya (UPC), Barcelona, 08034, Spain
[3]Associated Unit: Hydrogeology Group (UPC-CSIC)

Correspondence to: Mireia Fontanet (mireia@lab-ferrer.com)

Abstract. Soil moisture measurements are needed in a large number of applications such as hydro-climate approaches, watershed water balance management and irrigation scheduling. Nowadays, different kinds of methodologies exist for

10   measuring soil moisture. Direct methods based on gravimetric sampling or Time Domain Reflectometry (TDR) techniques measure soil moisture in a small volume of soil at few particular locations. This typically gives a poor description of the soil moisture spatial distribution in relatively large agriculture fields. Remote sensing of soil moisture provides a large coverage and can overcome this problem but suffers from other problems stemming from its low spatial resolution. In this context, the DISaggregation based on Physical And Theoretical scale CHange algorithm (DISPATCH) has been proposed in the

15   literature to downscale soil moisture satellite data from 40 km to 1 km of resolution by combining the low resolution Soil Moisture Ocean Salinity (SMOS) satellite soil moisture data with the high resolution (Normalized Difference Vegetation Index (NDVI) and Land Surface Temperature (LST) datasets obtained from a Moderate Resolution Imaging Spectroradiometer (MODIS) sensor. In this work, DISPATCH estimations are compared with soil moisture sensors and gravimetric measurements to validate the DISPATCH algorithm in an agricultural field during two different hydrologic

20   scenarios; wet conditions driven by rainfall events and local sprinkler irrigation. Results show that the DISPATCH algorithm provides appropriate soil moisture estimates during general rainfall events but not when sprinkler irrigation generates occasional heterogeneity. In order to explain these differences, we have examined the spatial variability scales of NDVI and LST data, which are the input variables involved in the downscaling process. Sample variograms show that the spatial scales associated with the NDVI and LST properties are too large to represent the variations of the average soil moisture at the site

25   and this could be a reason why the DISPATCH algorithm is not working properly in this field site.

1. Introduction

Soil moisture measurements taken over different spatial and temporal scales are increasingly required in a wide range of environmental applications, which include crop yield forecasting (Holzman et al., 2014), irrigation planning (Vellidis et al., 2016), early warnings for floods and draughts (Moriche and Rientjes, 2016), and weather forecasting (Dillon et al., 2016).

1

This is mostly due to the fact that soil moisture controls the water and energy exchange between key environmental compartments (atmosphere and earth) and hydrological processes, such as precipitation, evaporation, infiltration, and run-off (Ochsner, 2013; Robock et al., 2000).

There are several applications in which soil moisture measurements have been shown to provide relevant information (Robock et al., 2000). For example, in environmental applications, soil moisture is typically used for defining the water stress occurring in natural and human systems (Irmak et al., 2000) or for quantifying nitrate leaching and drainage quality (Clothier and Green, 1994). Here, we highlight that soil moisture measurements from the root zone yields important information for field irrigation scheduling, determining to a great extent the duration and frequency of irrigation needed for plant growth as a function of water availability (Blonquist et al., 2006; Jones, 2004; Campbell, 1982).

Soil moisture is highly variable in space and time, mainly as a result of the spatial variability in soil properties (Hawley, 1983), topography (Burt and Butcher, 1985), land uses (Fu, 1994), vegetation (Le Roux et al., 1995) and atmospheric conditions (Koster and Suarez, 2001). As a result, soil moisture data exhibits a strong scale effect that can substantially affect the reliability of predictions depending on the method of measurement used. For this reason, it is important to understand how to measure soil moisture for irrigation scheduling in a commercial field site.

Nowadays, available techniques for measuring or estimating soil moisture can provide data on a small or large scale. Gravimetric measurements (Gardner, 1986) estimate soil moisture by the difference between the natural and the dry weight of a given soil sample. They are used as a true value of soil moisture for sensor calibration (Starr and Paltineanu, 2002) or soil moisture validation studies (Bosch et al., 2006; Cosh et al., 2006). The main disadvantage of this method is that these measurements are time-consuming; users have to go to the field to collect soil samples and place them in the oven for a long time. Soil moisture sensors such as Time Domain Reflectometry sensors (Clarke Topp and Reynolds, 1998; Schaap et al., 2003; Topp et al., 1980) or capacitance sensors (Bogena et al., 2007; Dean et al., 1987) are capable of measuring soil moisture continuously using a data logger, thereby enabling the final user to save time. Soil moisture sensors are especially useful for studying processes at a small scale, but suffer from the fact that field data is typically scarce and provides an incomplete picture of a large area (Western et al., 1998). Nevertheless, the use of soil moisture sensors is a common practice

for guiding irrigation scheduling in cropping field systems (Fares and Polyakov, 2006; Thompson et al., 2007; Vellidis et al., 2008).

Remote Sensing, can estimate soil moisture continuously over large areas (Jackson et al., 1996). In this case, soil moisture estimations refer to the Near Surface Soil Moisture (NSSM), which represents the first 5 cm of the top soil profile. In recent years, Remote Sensing techniques have been improved and diversified their estimation, making them an interesting tool for monitoring NSSM and other variables such as the Normalized Difference Vegetation Index (NDVI) and the Land Surface Temperature (LST). Different satellites exist that are capable of estimating NSSM, one of them is the Soil Moisture and Ocean Salinity (SMOS) satellite launched in November 2009 (Kerr et al., 2001). It has global coverage and a revisit period of 3 days at the equator, giving two soil moisture estimations, the first one taken during the ascending overpass at 6:00 am and the second one during the descending overpass at 6:00 pm local solar time. SMOS satellite is a passive 2D interferometer operating at L-band (1.4 GHz) (Kerr et al., 2010). The spatial resolution ranges from 35 to 55 km, depending on the incident angle. Its goal is to retrieve NSSM with a target accuracy of a 0.04 m3/m3 (Kerr et al., 2012). Since SMOS NSSM have been validated on a regular basis since the beginning of its mission (Bitar et al., 2012; Delwart et al., 2008), it is considered suitable for hydro-climate applications (Lievens et al., 2015; Wanders et al., 2014).

The relatively large variability of soil moisture compared to the low resolution of SMOS-NSSM data hinders the direct application of this method to irrigation scheduling. However, the need for estimating NSSM with a resolution higher than 35 – 55 km using Remote Sensing has increased for different reasons: 1) This data can be downloaded easily from different web sites; 2) A field installation of soil moisture sensors is not necessary; and 3) No specific maintenance is needed. For these reasons, in the last few years, different algorithms have been developed to downscale Remote Sensing soil moisture data to tens or hundreds of meters.

Chauhan et al., (2003) developed a Polynomial fitting method which estimates soil moisture at 25 km resolution. This method links soil moisture data with surface temperature, vegetation index and albedo. It does not require in situ measurements but cannot be used under cloud coverage conditions. The change in the detection method reported by Narayan et al. (2006) downscales soil moisture at 100 m resolution. This is an optimal resolution for agricultural applications, but the method is highly dependent on the accuracy of its input data. The same problem is attributed to the Baseline algorithm for

the Soil Moisture Active Passive (SMAP) satellite (Das and Mohanty, 2006), which downscales soil moisture at 9 km resolution. These algorithms have to be validated using in situ measurements. For this purpose, most studies use soil moisture sensors installed at the top soil profile, i.e., the first 5 cm of soil (Albergel et al., 2011; Cosh et al., 2004; Jackson et al., 2010), while others use gravimetric soil moisture measurements (Merlin et al., 2012) or the combination of both

5   methodologies (Robock et al., 2000).

Other satellites, such as Sentinel-1, can estimate NSSM at 1 km resolution (Hornacek et al., 2012; Mattia et al., 2015; Paloscia et al., 2013). Sentinel-1 provides two kinds of products, the first one is Single Look Complex (SLC) and the second one is Ground Range Detected (GRD). The last one can be used for solving a wide range of problems related to Earth surface monitoring, such as soil moisture, but it is not a direct measurement and therefore data treatment is needed. In this

10 case, GRD product is converted into radar backscatter coefficient and then into dB units to estimate soil moisture. Usually, these conversations are cumbersome because these kind of measurements have surface roughness and vegetation influence that affect the signal (Garkusha et al., 2017; Wagner et al., 2010).

The DISPATCH method (DISaggagregation based on Physical And Theorical CHange) (Merlin et al., 2012; Merlin et al., 2008) is an algorithm that downscales SMOS NSSM data from 40 km (low resolution) to 1 km resolution (high resolution).

15 This algorithm uses Terra and Aqua satellite data to estimate NDVI and LST twice a day using the Moderate Resolution Imaging Spectroradiometer (MODIS) sensor. These estimations have 1 km resolution and can be conducted even if there is no cloud coverage. This downscaling process provides the final user with the possibility of estimating NSSM using Remote Sensing techniques at high resolution. DISPATCH succeed to reveal spatial heterogeneities as rivers, large irrigation areas and floods (Escorihuela and Quintana-Seguí, 2016; Malbéteau et al., 2015, 2017; Molero et al., 2016) and it has also been

20 validated (Malbéteau et al., 2015; Merlin et al., 2012; Molero et al., 2016) in fairly large and homogeneous irrigation areas, but not in complex settings with spatially changing hydrologic conditions such as those representing a local irrigation field.

In this work, we evaluate the worth Remote Sensing in agricultural irrigation scheduling by comparing in situ soil moisture data obtained from gravimetric and soil moisture sensors, with soil moisture data determined by downscaling Remote Sensing information with the DISPATCH algorithm.

1.1. Study Area

The study area shown in Figure 1 is located in the village of Foradada (1.015 lat., 41.866 lon.), in the Segarra – Garrigues (SG) system (Lleida, Catalonia). The SG system is an important hydraulic project currently being carried out in the province of Lleida, Catalonia, which involves converting most of the current dry land fields into irrigated fields. Its construction enables 1000 new hectares with a long agricultural tradition to be irrigated in most of the dry land. To achieve this, an 85 km long channel was constructed to supply water for irrigation. At present, approximately 16000 irrigators are potential beneficiaries of these installations. However, most farmers have not yet installed this irrigation system, which means that the SG systems can still be regarded as dry land.

The Urgell area is located in the west of the SG system. This area has totally different soil moisture conditions, especially during the summer season when the majority of fields are currently irrigated. This gives rise to two clearly distinguishable wet and dry soil moisture conditions. Figure 1 shows the Foradada field, which represents 25 ha of a commercial field irrigated by a solid set sprinkle irrigation system distributed with 18 different irrigation sectors. The soil texture is 65.6% Clay, 17.6% Silt and 16.8 Sand. Every year two different crops are grown, the first one during the winter and spring seasons, when wet conditions are maintained by precipitation, and the second one during the summer and autumn seasons, when wet conditions are maintained by sprinkler irrigation. The Foradada field is thus one of the few irrigated fields located within the SG system. Consequently, this field has soil moisture conditions similar to those in the surrounding area during the winter and spring season, but completely different conditions during the summer and autumn seasons. This makes this site unique for assessing Remote Sensing in a distinct isolated irrigation field.

2. Materials and Methods

2.1. In situ Soil Moisture Measurements

A total of 9 intensive and strategic field campaigns were conducted in the study area during 2016: DOY42, DOY85, DOY102, DOY187, DOY194, DOY200, DOY215, DOY221 and DOY224. During each field campaign, disturbed soil samples were collected from the top soil profile (0-5 cm depth) for measuring gravimetric soil moisture data. A total of 101 measurement points, depicted in Figure 1., were defined around the field. They are divided into two different kinds of points:

5

1) Cross section points; 75 points defined to represent the spatial variability of soil moisture in different cross sections. In these cross sections, points are separated by 9, 16 and 35 m; 2) Support points; 26 points complement information measured from cross sections, thereby adding and supporting information about soil spatial variability. Each soil sample is analyzed using the gravimetric method for measuring gravimetric soil moisture content, which is transformed to volumetric soil moisture content using bulk density measurements (Letelier, 1982). Daily averages and their standard deviations of gravimetric measurements were computed to represent the soil moisture associated with the entire field site.

Soil moisture was also measured using capacitive EC-5 sensors (METER Group, Pullman, WA, USA), previously calibrated in the laboratory (Star and Paltineanu, 2002). As Figure 1 shows, a total of 5 control points were installed across one of the three gravimetric cross sections. Each control point represents a different irrigation sector of the field. Soil moisture sensors were installed at 5 cm depth, taking into account the explore volume of these sensors. Their resolution is ±0.03 cm3·cm-3. They were connected to an EM50G data logger (METER Group, Pullman, WA, USA) that register soil moisture every 5 minutes.

2.2. DISPATCH Soil Moisture Measurements

In this section we briefly describe the DISPATCH algorithm. Further details can be found in Merlin et al. (2013) and references therein. The DISPATCH algorithm aims to downscale NSSM data obtained from SMOS at 40 km resolution to 1 km resolution. The method assumes that NSSM is a linear function of the Soil Evaporative Efficiency (SEE), which can be estimated at high resolution (1 km) from the acquisition of two products obtained from MODIS, i.e., LST and NDVI datasets. This MODIS-derived SEE is further considered as a proxy for the NSSM variability within the SMOS pixel. The estimation of SEE is assumed to be approximately constant during the day given clear sky conditions. The downscaling relationship is given by Eq. (1)

$$\theta_{HR} = \theta_{SMOS} + \theta'_{HR}(SEE_{SMOS}) \times (SEE_{HR} - SEE_{SMOS}), \tag{1}$$

where θ_{SMOS} is the low resolution SMOS soil moisture data, SEE_{HR} is the MODIS-derived SEE at a high resolution (1 km), SEE_{SMOS} is the average of SEE_{HR} within the SMOS pixel at a low resolution (40 km), and $\theta'_{HR}(SEE_{SMOS})$ is the partial derivative of soil moisture with respect to the soil evaporative efficiency at high resolution evaluated at the SEE_{SMOS} value.

This partial derivative is typically estimated by using the linear soil evaporative efficiency model of Budyko (1956) and Manabe (1969), which is written by Eq. (2)

$$\theta_{HR} = SEE_{HR} \times \theta_p \tag{2}$$

where θ_{HR} represents the soil moisture of the top soil layer (0-5 cm) at high resolution, and θ_p is an empirical parameter that depends on soil properties and atmospheric conditions. The soil evaporation efficiency at high resolution SEE_{HR} is estimated as a linear function of the soil temperature at high resolution ($T_{s,HR}$), Eq. (3)

$$SEE_{HR} = \frac{T_{s,max} - T_{s,HR}}{T_{s,max} - T_{s,min}}, \tag{3}$$

The soil temperature at high resolution is estimated by partitioning the MODIS surface temperature data (LST) into the soil and the vegetation component according to the trapezoid method of Moran et al. (1994). This also requires an estimation of the fractional vegetation cover, which is calculated from the NDVI data. $T_{s,min}$ and $T_{s,max}$ are the soil temperature end-members (Merlin et al., 2012).

In this work, the DISPATCH algorithm has been executed during period DOY36 and DOY298 to estimate NSSM at 1 km resolution in the Foradada field site. DISPATCH provides a daily NSSM pixel map (regular grid). The Foradada field site is entirely included in one pixel. In this pixel, 51.5% of the total area corresponds to irrigated area. The remaining portion of the pixel corresponds to dry land (shown in Figure 2).

2.3. Image Spatial Resolution and Spatial Variability

The information contained in a satellite image is characterized here by two properties: the spatial resolution and the spatial variability of the image attributes. The spatial resolution of a satellite image is the ground area represented by each pixel, i.e., the raster cell size. It is essentially the representative support volume chosen to describe the variations of the attributes of interest at the ground. This is typically determined based on the type of satellite sensor. Instead, the spatial variability refers to the variations of the attributes presented in the image at the ground surface, e.g., patterns of spatial continuity, size of objects in the scene, and so on. In random field theory and geostatistics, the spatial variability is mainly characterized by the covariance function or by its equivalent, the semivariogram, which is defined by (Journel and Huijbregts, 1978) Eq. (4),

$$\gamma(h) = \frac{1}{2} E\{[Z(x+h) - Z(x)]^2\}, \tag{4}$$

7

where Z(x) is the random variable at the x position, and E{·} is the expectation operator. Essentially, the semivariogram is a function that measures the variability between pairs of variables separated by a distance h. Very often, the correlation between two variables separated by a certain distance disappears when |h| becomes too large. At this instant, $\gamma(h)$ approaches a constant value. The distance beyond which $\gamma(h)$ can be considered to be a constant value is known as the

5   range, which represents the transition of the variable to the state of negligible correlation. Thus, the range can ultimately be seen as the size of independent objects in the image. If the pixel size is smaller than 10 times the minimum range (in the absence of the nugget effect), then neighbour pixels will be alike, containing essentially the same level of information (Journel and Huijbregts, 1978). This will be a critical point in the discussion of the results later on. We finally note that the spatial resolution and the spatial variability are two related concepts. Several authors content that a rational choice of the

10   spatial resolution for remote sensing should be based on the relationship between spatial resolution and spatial dependence. However, since this is not the usual procedure, the spatial resolution can be inappropriate in some cases or provide unnecessary data (Atkinson and Curran, 1997; Woodcock and Strahler, 1987).

3. Results

3.1. General Observations

15   One of the main advantages of our experiment is that remote sensing soil moisture data is evaluated during two different hydrologic periods of the same year in a given agriculture field site. The first period represents crop growth with soil wet conditions caused by natural rainfall events (without irrigation). This period transpired during the winter and spring season, i.e., from February to June. The following period occurs during the dry season with artificially created soil wet conditions caused by sprinkler irrigation operating upon crop demand during the summer and autumn season, from June to October. In

20   contrast to the rainfall events, sprinkler irrigation creates a local artificial rainfall event using several rotating sprinkler heads. The comparisons of these two hydrologic periods allow us to evaluate the sole effect of local sprinkler irrigation on remote sensing estimates.

Figures 3 compares gravimetric and soil moisture sensor measurements with the DISPATCH soil moisture estimates obtained from remote sensing data during the first period of time (without irrigation). We note that the comparison here is

8

not between punctual gravimetric measurements (with support volume of few centimetres) and satellite information (1 km in resolution). compare the average of these punctual measurements over the entire field site (very well distributed with more than 100 measurement points) with satellite information. The average of the soil moisture is representative of the entire irrigated area associated with the Foradada field site. Consequently, these two variables have similar support scale and are

5   therefore comparable. Error bars in the gravimetric measurements represent the standard deviation of all the measurements obtained in one day. In addition, the green region in this figure displays the daily minimum and maximum values of soil moisture data obtained from EC-5 sensors. We note that the average of gravimetric soil moisture data lays always within this region. Therefore, this information can be used to complement soil moisture data in days where no gravimetric sampling is available. The error bars associated with DISPATCH data refer to the standard deviation obtained with two daily SMOS

10   estimations and four MODIS data (two at 6:00am and two more at 6:00 pm). To better appreciate tendencies, the same information is also presented as a normalized relative soil moisture, i.e., $(\theta - \theta_{min})/(\theta_{max} - \theta_{min})$, where θ_{min} are the minimum and maximum values of all soil moisture measurements. results show that DISPATCH estimates can properly detect the relative increase in soil moisture estimates caused by general rainfall events. Note for instance that all methods produce a similar relative increase in soil moisture signal after the occurrence of a strong rainfall event. In absolute terms, we

15   see that DISPATCH can slightly underestimate the true value of soil moisture but this could be attributed to small differences between the support volume of the field site and the spatial resolution of the satellite image.

A similar analysis is shown in Figure 4, which compares gravimetric and sensor soil moisture measurements with DISPATCH soil moisture estimations during the second period (soil wet conditions maintained by sprinkler irrigation). In contrast to our previous results, one can see that the DISPATCH dataset is essentially not sensitive to sprinkler irrigation

20   even though they respond properly to sporadic small rainfall events. Likewise, the relative increase in soil moisture measurements also shows that sprinkler irrigation does not affect the DISPATCH estimation. Thus, even though the DISPATCH estimations seems to properly respond to significant rainfall events during the first period, irrigation operating at the Foradada field scale remains undetected during the second period. The DISPATCH dataset disregards irrigation and merely indicates that soil dry conditions exist at a larger picture. We conclude then that the DISPATCH dataset provides

25   representative estimates of soil moisture at a resolution lower than expected.

3.2. Analysis and Discussion

We seek to answer the important question of why the DISPATCH soil moisture estimates obtained by downscaling satellite information from 40 km to 1 km of resolution are not sensitive to sprinkler irrigation in this case. The following possible sources of discrepancies can be identified: (i) errors associated with the approximations used in the DISPATCH downscaling formulation; (ii) differences in the scale of observations; and (iii) low quality of information associated with DISPATCH input variables. We concentrate the analysis on (ii) and (iii). First, we note that the DISPATCH resolution of 1 km is similar to the characteristic scale of the irrigated area at the Foradad field site and therefore a better performance was expected. The extent of the irrigated area in the DISPATCH pixel size of interest is 51.5 % (see Figure 2). Given that soil moisture is a linear property, we contend that this cannot explain the almost zero relative increase in soil moisture obtained during irrigation. Then, we examine the semivariograms of the different input variables involved in the downscaling process, i.e., the NDVI and the LST properties provided by the MODIS sensor. The NDVI and LST semivariograms were respectively estimated from the MOD13A2 and MOD11A1 product data, which can be freely downloaded from the Google Earth Engine website (https://earthengine.google.com). We selected a daily representative image of April, June and August. The April image describes a general rainfall event in the region, the June image shows when local irrigation starts in the Foradada field, and finally the August image represents when the crop is well developed and frequent irrigation is needed. Experimental semivariograms have been fitted with a theoretical model (spherical and exponential models for the LST and NDVI, respectively), which can be formally expressed as Eq. 5 and 6,

$$\gamma_{LST}(h) = c_{11} \, Sph\left(\frac{|h|}{a_{11}}\right) + c_{12}\left[1 - \cos\left(\frac{|h|}{a_{12}}\,\pi\right)\right], \tag{5}$$

$$\gamma_{NDVI}(h) = c_{21} \, Exp\left(\frac{|h|}{a_{21}}\right) + c_{22} \, Exp\left(\frac{|h|}{a_{22}}\right) + c_{23}\left[1 - \cos\left(\frac{|h|}{a_{23}}\,\pi\right)\right], \tag{6}$$

where c_{ij} are constant coefficients that represent the contribution of the different standard semivariogram models, and a_{ij} are the corresponding ranges of the different structures. The LST and NDVI experimental and theoretical semivariograms are shown in Figure 5. The parameters adopted in the random function model are summarized in Tables 1 and 2. The analysis determines a nested structure with a positive linear combination between isotropic stationary semivariogram models and the hole effect model. Hole effect structures most often indicate a form of periodicity (Pyrcz and Deutsch, 2003). In our case,

this periodicity reflects the presence of areas with different watering and crop growth conditions, i.e., in contrast to the SG area, the Urgell area is based on irrigation.

The spatial variability of NDVI and LST vary with time according to changes in hydrologic conditions. In April, the semivariogram of NDVI displays more variability and less spatial continuity due to the differences in growth rate and crop

5 type conditions existing at the regional scale during the wet season (controlled by rainfall events). On the other hand, the spatial dependence of LST is more significant in August. Importantly, results show that the scale of variability (range) associated with MODIS data during the dry season, when a controlled amount of water by irrigation is applied, ranges between 35 and 36 km for the NDVI and between 22 and 32 km for the LST. Recalling the discussion provided in section 2.3., this means that the size of independent objects in the NDVI and LST images is about 30 kms and that insignificant

10 spatial variations of NDVI and LST values are expected below 1/ of this size. This suggests that the NDVI and LST products provided by MODIS cannot detect differences between neighbour pixels of size 1 km.

To further corroborate this point, Figure 6 compares the temporal evolution of LST and NDVI obtained from two aligh MODIS pixels: the Foradada pixel and its North-West neighbour pixel. Note that the neighbour pixel corresponds to a not irrigated . Data was downloaded using MOD13A2 and MOD11A1 products with Google Earth Engine website, from

15 DOY036 to DOY298. In general, irrigation in an agriculture field site should produce a decrease in LST values and an increase in NDVI. However, Figure 6 shows the same dynamics and similar values in both pixels even when irrigation is applied. Results show that the LST and NDVI information cannot detect neither the sprinkler irrigation nor the crop growth as a consequence of irrigation in this case.

4. Conclusions

20 We analyze the value of Remote Sensing and the DISPATCH downscaling algorithm for predicting soil moisture variations in an irrigated field site of size close to image resolution. The DISPATCH algorithm based on the NDVI and LST data obtained from the MODIS satellite is used for downscaling the SMOS information and transforming the SMOS soil moisture estimations from a resolution of 40 km to 1 km. These estimates are then compared with average gravimetric and soil moisture sensors measures taken all over the field site. Results have shown that in this case the downscaled soil moisture

11

estimations are capable of predicting the variations in soil moisture caused by general rainfall events but fail to reproduce the temporal fluctuations of the average water content caused by local irrigation. To provide insight into this problem, we examine the spatial variability of the different input variables involved, i.e., the NDVI, the LST. Results indicated that the size of individual objects in the NDVI and LST images is too large to be able to represent adequately the variations of the

5   average water content at the site. This effect is not significant during rainfall events because the typical spatial scale of rainfall events is much larger than the size of the irrigated field site.

From a different perspective, these results also suggest that irrigation scheduling based on satellite information coupled with the DISPATCH downscaling algorithm can be appropriate in regions of the world with extensive irrigation surface coverage, larger than approximately 10 km (e.g., Punjab basin). However, caution should be paid to the direct application of this

10   method as its performance will strongly depend on the spatiotemporal variation of the irrigation within the area. These variations can generate occasional heterogeneity leading to the failure of the soil moisture prediction method.

References

Albergel, C., Rosnay, P. De, Gruhier, C., Muñoz-sabater, J., Hasenauer, S., Isaksen, L., Kerr, Y. and Wagner, W.: in Situ Observations, 2011.

15   Atkinson, P. and Curran, P.: Choosing an appropriate spatial resolution for remote sensing investigations, Photogramm. Eng. Remote Sens., 63(12), 1345–1351 [online] Available from: http://asprs.org/a/publications/pers/97journal/december/1997_dec_1345-1351.pdf, 1997.

Bitar, A. Al, Leroux, D., Kerr, Y. H., Member, S., Merlin, O., Richaume, P., Sahoo, A. and Wood, E. F.: Evaluation of SMOS Soil Moisture Products Over Continental U . S . Using the SCAN / SNOTEL Network, IEEE Trans. Geosci. Remote

20   Sens., 50(5), 1572–1586, doi:10.1109/TGRS.2012.2186581, 2012.

Blonquist, J. M., Jones, S. B. and Robinson, D. A.: Precise irrigation scheduling for turfgrass using a subsurface electromagnetic soil moisture sensor, Agric. Water Manag., 84(1–2), 153–165, doi:10.1016/j.agwat.2006.01.014, 2006.

Bogena, H. R., Huisman, J. A., Oberdörster, C. and Vereecken, H.: Evaluation of a low-cost soil water content sensor for wireless network applications, J. Hydrol., 344(1–2), 32–42, doi:10.1016/j.jhydrol.2007.06.032, 2007.

25   Bosch, D. D., Lakshmi, V., Jackson, T. J., Choi, M. and Jacobs, J. M.: Large scale measurements of soil moisture for validation of remotely sensed data: Georgia soil moisture experiment of 2003, J. Hydrol., 323(1–4), 120–137, doi:10.1016/j.jhydrol.2005.08.024, 2006.

Budyko, M. I. (1956). Heat balance of the Earth's surface. Leningrad.

Burt, T. P. and Butcher, D. P.: Topographic controls of soil moisture distributions, J. Soil Sci., 36(3), 469–486, doi:10.1111/j.1365-2389.1985.tb00351.x, 1985.

Chauhan, N. S., Miller, S. and Ardanuy, P.: Spaceborne soil moisture estimation at high resolution: A microwave-optical/IR synergistic approach, Int. J. Remote Sens., 24(22), 4599–4622, doi:10.1080/0143116031000156837, 2003.

5   Clarke Topp, G. and Reynolds, W. D.: Time domain reflectometry: A seminal technique for measuring mass and energy in soil, Soil Tillage Res., 47(1–2), 125–132, doi:10.1016/S0167-1987(98)00083-X, 1998.

Clothier, B. E. and Green, S. R.: Rootzone processes and the efficient use of irrigation water, Agric. Water Manag., 25(1), 1–12, doi:10.1016/0378-3774(94)90048-5, 1994.

Cosh, M. H., Jackson, T. J., Bindlish, R. and Prueger, J. H.: Watershed scale temporal and spatial stability of soil moisture
10   and its role in validating satellite estimates, Remote Sens. Environ., 92(4), 427–435, doi:10.1016/j.rse.2004.02.016, 2004.

Cosh, M. H., Jackson, T. J., Starks, P. and Heathman, G.: Temporal stability of surface soil moisture in the Little Washita River watershed and its applications in satellite soil moisture product validation, J. Hydrol., 323(1–4), 168–177, doi:10.1016/j.jhydrol.2005.08.020, 2006.

Das, N. N. and Mohanty, B. P.: Root Zone Soil Moisture Assessment Using Remote Sensing and Vadose Zone Modeling,
15   Vadose Zo. J., 5(1), 296, doi:10.2136/vzj2005.0033, 2006.

Dean, T. J., Bell, J. P. and Baty, A. J. B.: Soil moisture measurement by an improved capacitance technique, Part I. Sensor design and performance, J. Hydrol., 93(1–2), 67–78, doi:10.1016/0022-1694(87)90194-6, 1987.

Delwart, S., Bouzinac, C., Wursteisen, P., Berger, M., Drinkwater, M., Martín-Neira, M. and Kerr, Y. H.: SMOS validation and the COSMOS campaigns, IEEE Trans. Geosci. Remote Sens., 46(3), 695–703, doi:10.1109/TGRS.2007.914811, 2008.

20   Dillon, M. E., Collini, E. A. and Ferreira, L. J.: Sensitivity of WRF short-term forecasts to different soil moisture initializations from the GLDAS database over South America in March 2009, Atmos. Res., 167, 196–207, doi:10.1016/j.atmosres.2015.07.022, 2016.

Escorihuela, M. J. and Quintana-Seguí, P.: Comparison of remote sensing and simulated soil moisture datasets in Mediterranean landscapes, Remote Sens. Environ., 180, 99–114, doi:10.1016/j.rse.2016.02.046, 2016.

25   Fares, A. and Polyakov, V.: Advances in Crop Water Management Using Capacitive Water Sensors, Adv. Agron., 90(May 2014), 43–77, doi:10.1016/S0065-2113(06)90002-9, 2006.

Fu, B. and H. G.: Land evaluations in an areaof severe erosion: the loess plateau of China, L. Degrad. Rehabil.l. Degrad. Rehabil., 5:33-40(February), 33–40 [online] Available from: f, 1994.

Garkusha, I. N., Hnatushenko, V. V. and Vasyliev, V. V.: Using Sentinel-1 data for monitoring of soil moisture, 2017 IEEE
30   Int. Geosci. Remote Sens. Symp., (July), 1656–1659, doi:10.1109/IGARSS.2017.8127291, 2017.

Hawley: Journal of Hydrology, 62 (1983) 179--200, J. Hydrol., 62, 179–200, doi:10.1016/0022-1694(83)90102-6, 1983.

Holzman, M. E., Rivas, R. and Piccolo, M. C.: International Journal of Applied Earth Observation and Geoinformation Estimating soil moisture and the relationship with crop yield using surface temperature and vegetation index, , 28, 181–192, 2014.

Hornacek, M., Wagner, W., Sabel, D., Truong, H.-L., Snoeij, P., Hahmann, T., Diedrich, E. and Doubkova, M.: Potential for High Resolution Systematic Global Surface Soil Moisture Retrieval via Change Detection Using Sentinel-1, IEEE J. Sel. Top. Appl. Earth Obs. Remote Sens., 5(4), 1303–1311, doi:10.1109/JSTARS.2012.2190136, 2012.

Irmak, S., Haman, D. Z. and Bastug, R.: Determination of crop water stress index for irrigation timing and yield estimation of corn, Agron. J., 92(6), 1221–1227, doi:10.2134/agronj2000.9261221x, 2000.

Jackson, T. J., Schugge, J. and Engman, E. T.: Remote sensing applications to hydrology: soil moisture, Hydrol. Sci. J., 41(4), 517–530, doi:10.1080/02626669609491523, 1996.

Jackson, T. J., Cosh, M. H., Bindlish, R., Starks, P. J., Bosch, D. D., Seyfried, M., Goodrich, D. C., Moran, M. S. and Du, J.: Validation of advanced microwave scanning radiometer soil moisture products, IEEE Trans. Geosci. Remote Sens., 48(12), 4256–4272, doi:10.1109/TGRS.2010.2051035, 2010.

Jones, H. G.: Irrigation scheduling: Advantages and pitfalls of plant-based methods, J. Exp. Bot., 55(407), 2427–2436, doi:10.1093/jxb/erh213, 2004.

Kerr, Y. H., Waldteufel, P., Wigneron, J. P., Martinuzzi, J. M., Font, J. and Berger, M.: Soil moisture retrieval from space: The Soil Moisture and Ocean Salinity (SMOS) mission, IEEE Trans. Geosci. Remote Sens., 39(8), 1729–1735, doi:10.1109/36.942551, 2001.

Kerr, Y. H., Waldteufel, P., Wigneron, J., Delwart, S., Cabot, F., Font, J., Reul, N., Boutin, J., Gruhier, C., Juglea, S. E., Drinkwater, M. R., Mecklenburg, S., Hahne, A. and Martı, M.: The SMOS Mission : New Tool for Monitoring Key Elements of the Global Water Cycle, , 98(5), 2010.

Kerr, Y. H., Waldteufel, P., Richaume, P., Wigneron, J. P., Ferrazzoli, P., Mahmoodi, A., Bitar, A. Al, Cabot, F., Gruhier, C., Juglea, S. E., Leroux, D., Mialon, A. and Delwart, S.: The SMOS Soil Moisture Retrieval Algorithm, Geosci. Remote Sens., 50(5), 1384–1403, doi:10.1109/TGRS.2012.2184548, 2012.

Koriche, S. A. and Rientjes, T. H. M.: Application of satellite products and hydrological modelling for flood early warning, Phys. Chem. Earth, 93, 12–23, doi:10.1016/j.pce.2016.03.007, 2016.

Koster, R. D. and Suarez, M. J.: Soil Moisture Memory in Climate Models, J. Hydrometeorol., 2(6), 558–570, doi:10.1175/1525-7541(2001)002<0558:SMMICM>2.0.CO;2, 2001.

Lievens, H., Tomer, S. K., Al Bitar, A., De Lannoy, G. J. M., Drusch, M., Dumedah, G., Hendricks Franssen, H. J., Kerr, Y. H., Martens, B., Pan, M., Roundy, J. K., Vereecken, H., Walker, J. P., Wood, E. F., Verhoest, N. E. C. and Pauwels, V. R. N.: SMOS soil moisture assimilation for improved hydrologic simulation in the Murray Darling Basin, Australia, Remote Sens. Environ., 168, 146–162, doi:10.1016/j.rse.2015.06.025, 2015.

Malbéteau, Y., Merlin, O., Molero, B., Rüdiger, C. and Bacon, S.: DisPATCh as a tool to evaluate coarse-scale remotely sensed soil moisture using localized in situ measurements: Application to SMOS and AMSR-E data in Southeastern Australia, Int. J. Appl. Earth Obs. Geoinf., 45(January 2015), 221–234, doi:10.1016/j.jag.2015.10.002, 2015.

Malbéteau, Y., Merlin, O., Balsamo, G., Er-Raki, S., Khabba, S., Walker, J. P. and Jarlan, L.: Towards a surface soil moisture product at high spatio-temporal resolution: temporally-interpolated spatially-disaggregated SMOS data, J.

Hydrometeorol., JHM-D-16-0280.1, doi:10.1175/JHM-D-16-0280.1, 2017.

Mattia, F., Satalino, G., Balenzano, A., Rinaldi, M., Steduto, P. and Moreno, J.: SENTINEL-1 FOR WHEAT MAPPING AND SOIL MOISTURE RETRIEVAL, IGARSS, 2(1), 2832–2835, 2015.

Manabe, S. (1969). Climate and the ocean circulation. I. The atmospheric circulation and the hydrology of the Earth's surface. Monthly Weather Review, 97(11), 739–774.

Merlin, O., Chehbouni, G., Walker, J. P., Panciera, R., Kerr, Y. H., Merlin, O., Chehbouni, G., Walker, J. P., Panciera, R. and Kerr, Y. H. A.: A simple methods for downscaling passive microwave based soil moisture Passive microwave soil moisture downscaling using evaporative fraction Olivier Merlin Abdelghani Chehbouni Jeffrey P . Walker Rocco Panciera Yann Kerr Centre d ' Etudes Spatiales de la, IEEE Geosci. Remote Sens. Lett., 46, 786–769, 2008.

Merlin, O., Jacob, F., Wigneron, J. P., Walker, J. and Chehbouni, G.: Multidimensional disaggregation of land surface temperature using high-resolution red, near-infrared, shortwave-infrared, and microwave-L bands, IEEE Trans. Geosci. Remote Sens., 50(5 PART 2), 1864–1880, doi:10.1109/TGRS.2011.2169802, 2012.

Merlin, O., Stefan, V., Malbéteau, Y., Escorihuela, M.-J., Rüdiger, C. and Jarlan, L.: Data disaggregation and evapotranspiration modeling: a synergism between multi-spectral/multi-resolution remote sensing data, Am. Geophys. Union, 2013.

Molero, B., Merlin, O., Malbéteau, Y., Al Bitar, A., Cabot, F., Stefan, V., Kerr, Y., Bacon, S., Cosh, M. H., Bindlish, R. and Jackson, T. J.: SMOS disaggregated soil moisture product at 1 km resolution: Processor overview and first validation results, Remote Sens. Environ., 180, 361–376, doi:10.1016/j.rse.2016.02.045, 2016.

Narayan, U., Lakshmi, V. and Jackson, T. J.: High resolution estimation of soil moisture using L-band radiometer and radar observations made during trhe SMEX02 experiments, IEEE Trans. Geosci. Remote Sens., 44(6), 1545–1554, 2006.

Ochsner, et al.: State of the art in large-scale soil moisture monitoring, Soil Sci. Soc. Am. Journal, Soil Sci. Soc. Am., 2013.

Paloscia, S., Pettinato, S., Santi, E., Notarnicola, C., Pasolli, L. and Reppucci, A.: Soil moisture mapping using Sentinel-1 images: Algorithm and preliminary validation, Remote Sens. Environ., 134(February 2015), 234–248, doi:10.1016/j.rse.2013.02.027, 2013.

Pyrcz, M. and Deutsch, C.: The whole story on the hole effect, Geostatistical Assoc. Australas. Newsl. 18, 18, 18 [online] Available from: http://www.gaa.org.au/pdf/gaa_pyrcz_deutsch.pdf, 2003.

Robock, A., Vinnikov, K. Y., Srinivasan, G., Entin, J. K., Hollinger, S. E., Speranskaya, N. A., Liu, S. and Namkhai, A.: The Global Soil Moisture Data Bank, Bull. Am. Meteorol. Soc., 81(6), 1281–1299, doi:10.1175/1520-0477(2000)081<1281:TGSMDB>2.3.CO;2, 2000.

Le Roux, X., Bariac, T. and Mariotti, a: Spatial partitioning of the soil water resoucre between grasses and shrub compnents in a west African humid savanna., Oecologia, 104, 145–155, doi:10.1007/BF00328579, 1995.

Schaap, M. G., Robinson, D. a., Friedman, S. P. and Lazar, a.: Measurement and Modeling of the TDR Signal Propagation through Layered Dielectric Media, Soil Sci. Soc. Am. J., 67(4), 1113, doi:10.2136/sssaj2003.1113, 2003.

Thompson, R. B., Gallardo, M., Valdez, L. C. and Fernández, M. D.: Using plant water status to define threshold values for

irrigation management of vegetable crops using soil moisture sensors, Agric. Water Manag., 88(1–3), 147–158, doi:10.1016/j.agwat.2006.10.007, 2007.

Topp, G. C., Davis, J. L. and Annan, A. P.: Electromagnetic Determination of Soil Water Content: Measruements in Coaxial Transmission Lines, Water Resour. Res., 16(3), 574–582, doi:10.1029/WR016i003p00574, 1980.

5 Vellidis, G., Tucker, M., Perry, C., Kvien, C. and Bednarz, C.: A real-time wireless smart sensor array for scheduling irrigation, Comput. Electron. Agric., 61(1), 44–50, doi:10.1016/j.compag.2007.05.009, 2008.

Vellidis, G., Liakos, V., Perry, C., Porter, W. M. and Tucker, M. A.: Irrigation Scheduling for Cotton Using Soil Moisture Sensors, Smartphone Apps, and Traditional Methods, , 772–780 [online] Available from: http://vellidis.org/wp-content/uploads/2016/07/Vellidis-Beltwide-Paper-16779-Irrigation-Scheduling.pdf, 2016.

10 Wagner, W., Sabel, D., Doubkova, M., Bartsch, A. and Pathe, C.: The Potential of Sentinel-1 for Monitoring Soil Moisture with a high Spatial Resolution at Global Scale, ESA Spec. Publ. SP-674, 5, 2010.

Wanders, N., Karssenberg, D., De Roo, A., De Jong, S. M. and Bierkens, M. F. P.: The suitability of remotely sensed soil moisture for improving operational flood forecasting, Hydrol. Earth Syst. Sci., 18(6), 2343–2357, doi:10.5194/hess-18-2343-2014, 2014.

15 Western, A. W., Blöschl, G. and Grayson, R. B.: Geostatistical characterisation of soil moisture patterns in the Tarrawarra catchment, J. Hydrol., 205(1–2), 20–37, doi:10.1016/S0022-1694(97)00142-X, 1998.

Woodcock, C. E. and Strahler, A. H.: the Factor of Scale in Remote-Sensing, Remote Sens. Environ., 21(3), 311–332, doi:10.1016/0034-4257(87)90015-0, 1987.
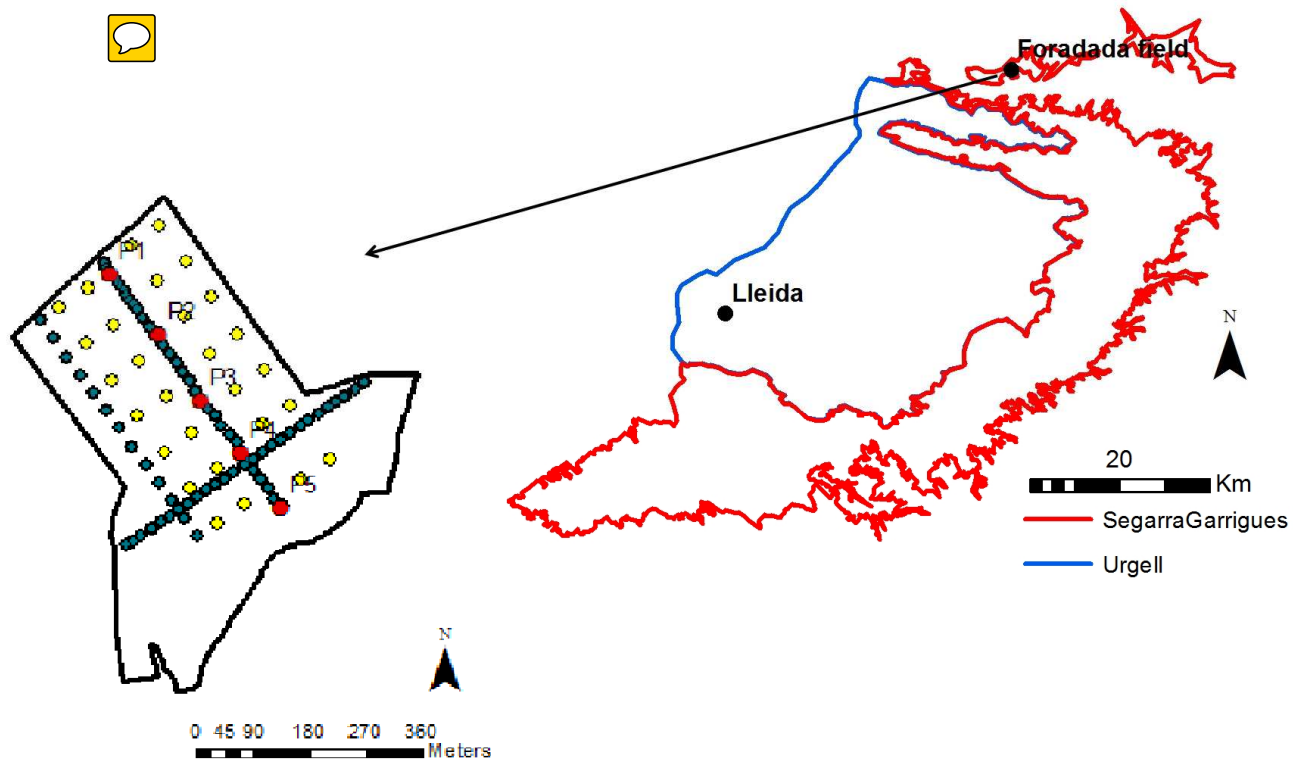
20 **Figures**

16

Figure 1. Location of the Foradada field site within the Segarra-Garriga irrigation system and distribution of soil moisture measurement points. Gravimetric measurement points are arranged with cross section points in green and support points in yellow. The location of EC-5 sensors are represented in red.

5

Figure 2. The DISPATCH grid representing the Foradada field, outlined in dark blue; irrigated fields, in light blue; and dry land in light red.

Figure 3. Comparison of average gravimetric soil moisture measurements (red) with the DISPATCH soil moisture estimations (yellow) and the daily maximum and minimum soil moisture sensors measurements (green) during the first hydrologic period (soil wet conditions caused by rainfall events only).
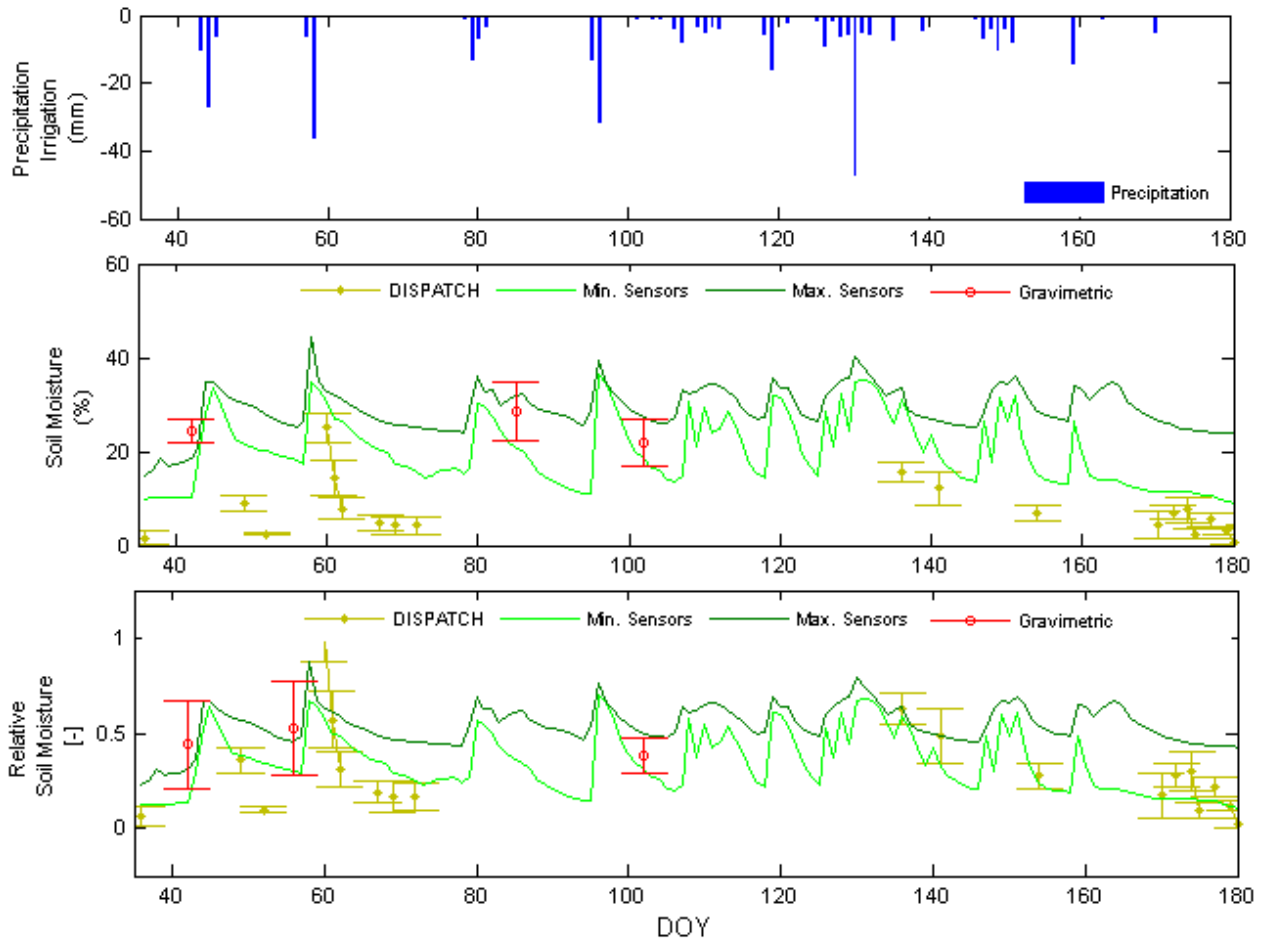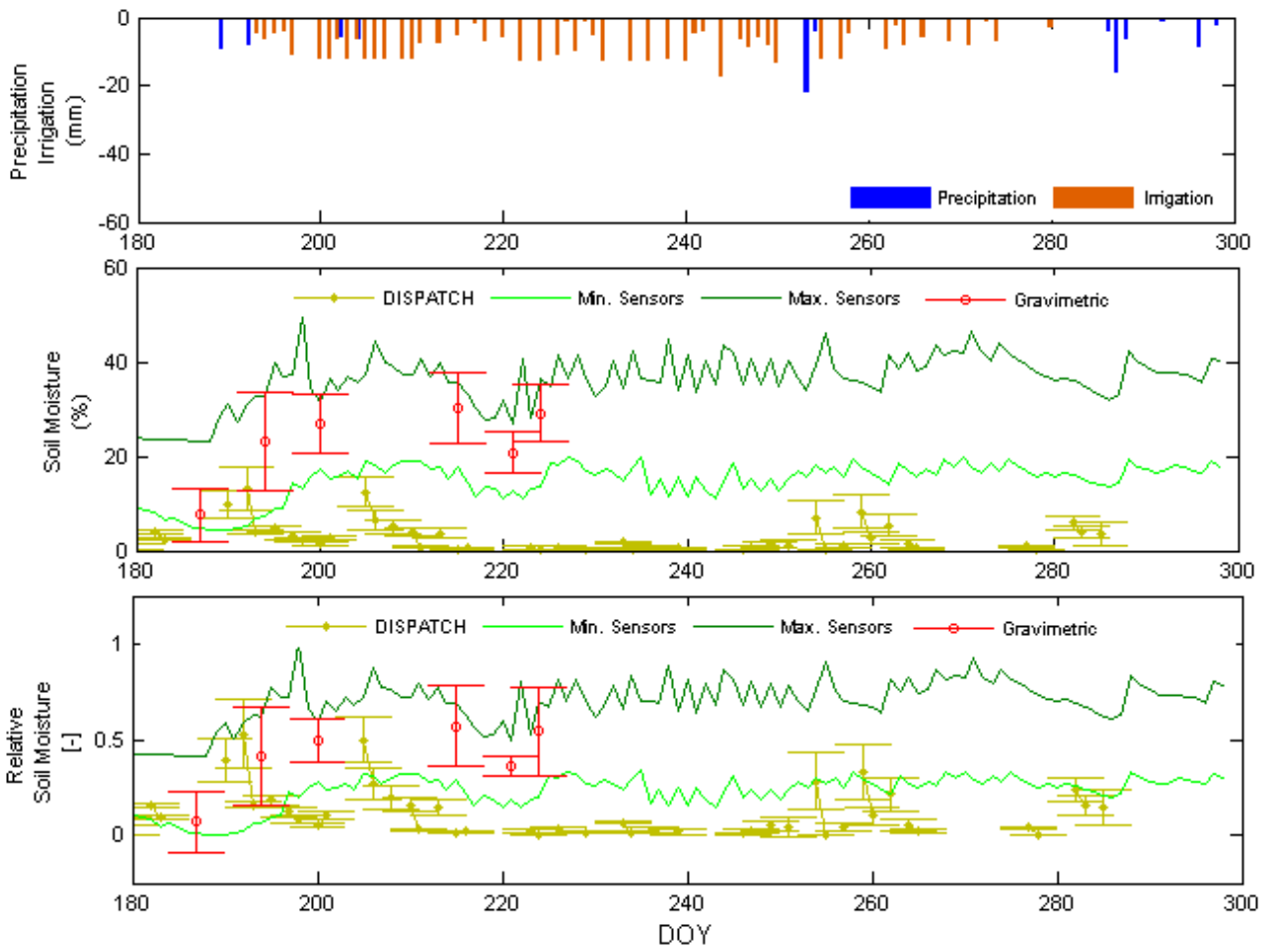
19

Figure 4. Comparison of average gravimetric soil moisture measurements (red) with the DISPATCH soil moisture estimations (yellow) and the daily maximum and minimum soil moisture sensors measurements (green) during the second hydrologic period (soil wet conditions caused by irrigation). The top figure shows the intensity of precipitation and irrigation.
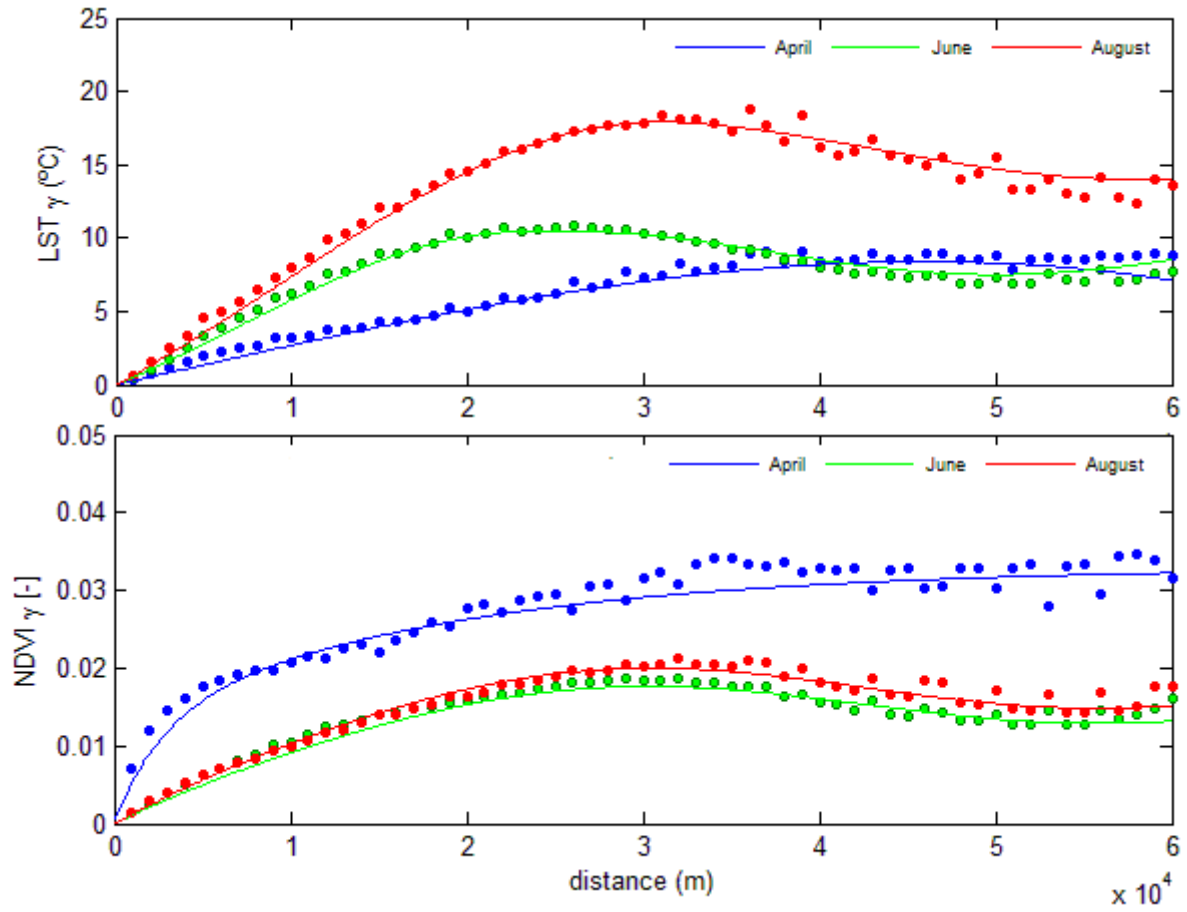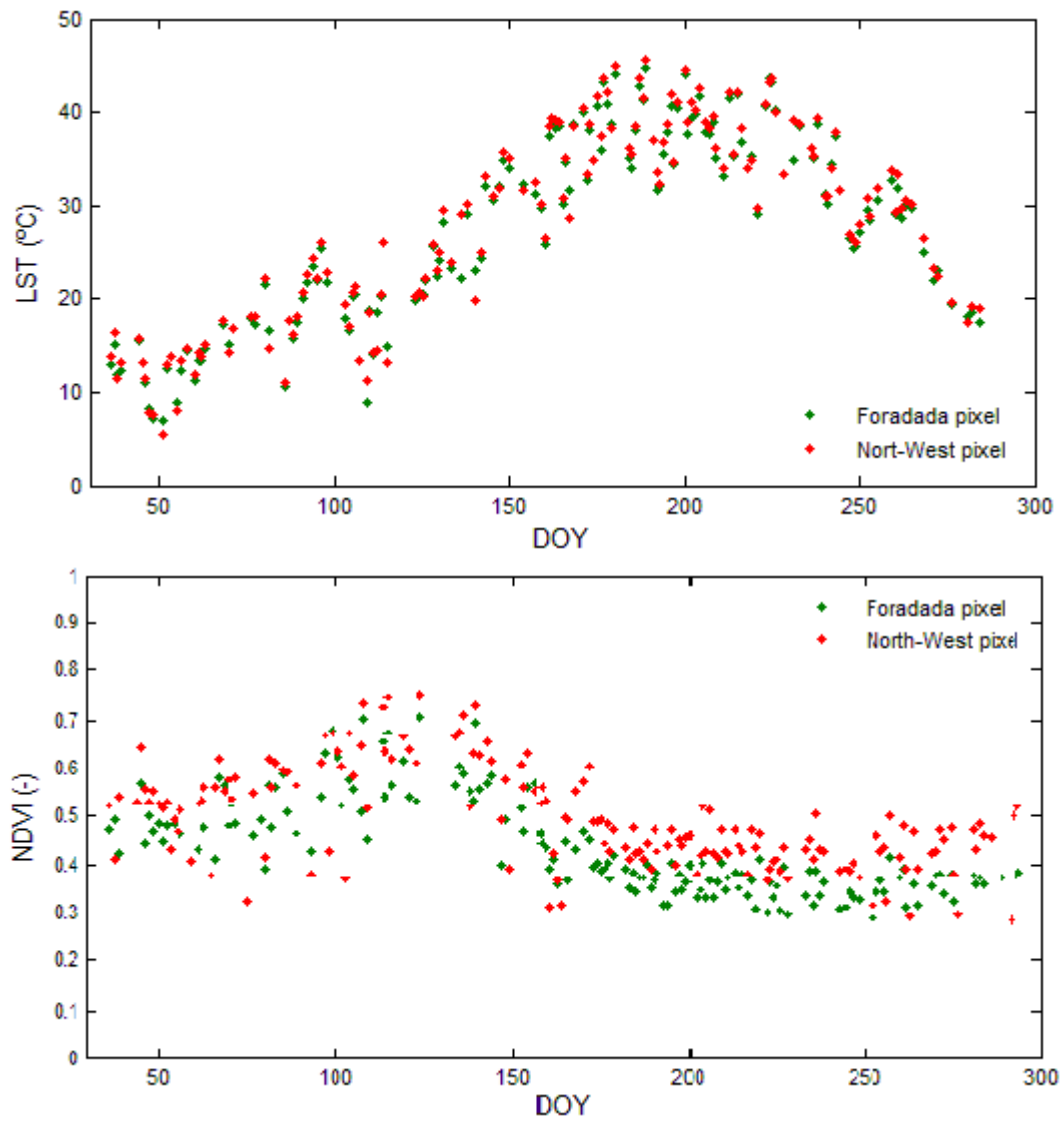
Figure 5. LST and NDVI experimental and theoretical semivariograms associated with April (blue), June (green), and August (red).

Figure 6. Temporal evolution of LST and NDVI obtained at the Foradada pixel and its neighbour North-West pixel situated 2 kms away.

Tables

<table>
<tr><td colspan="6">LST</td></tr>
<tr><td></td><td></td><td colspan="2">Variogram</td><td colspan="2">Hole effect</td></tr>
<tr><td>Month</td><td>Model</td><td>Sill (c_{11})</td><td>Range (a_{11})</td><td>Sill (c_{12})</td><td>Range (a_{12})</td></tr>
<tr><td>April</td><td>Spheric</td><td>8.4</td><td>46000</td><td>-</td><td>-</td></tr>
<tr><td>June</td><td>Spheric</td><td>7.5</td><td>22000</td><td>1.5</td><td>25000</td></tr>
<tr><td>August</td><td>Spheric</td><td>14</td><td>32000</td><td>2</td><td>29000</td></tr>
</table>

Table 1. Randon function model parameters of LST semivariograms.

5

<table>
<tr><td colspan="8">NDVI</td></tr>
<tr><td></td><td></td><td colspan="4">Variogram</td><td colspan="2">Hole effect</td></tr>
<tr><td>Month</td><td>Model</td><td>Sill (c_{21})</td><td>Range (a_{21})</td><td>Sill (c_{22})</td><td>Range (a_{22})</td><td>Sill (c_{23})</td><td>Range (a_{23})</td></tr>
<tr><td>April</td><td>Exponential</td><td>0.013</td><td>8000</td><td>0.02</td><td>55000</td><td>-</td><td>-</td></tr>
<tr><td>June</td><td>Exponential</td><td>0.013</td><td>35000</td><td>-</td><td>-</td><td>0.22</td><td>28000</td></tr>
<tr><td>August</td><td>Exponential</td><td>0.015</td><td>36000</td><td>-</td><td>-</td><td>0.21</td><td>28000</td></tr>
</table>

Table 2. Random function model parameters of NDVI semivariograms.